ORGANOMETALLICS

pubs.acs.org/Organometallics Article

Investigation of Iron Silyl Complexes as Active Species in the Catalytic Hydrosilylation of Aldehydes and Ketones

C. Vance Thompson, Hadi D. Arman, and Zachary J. Tonzetich*



Cite This: Organometallics 2022, 41, 430–440



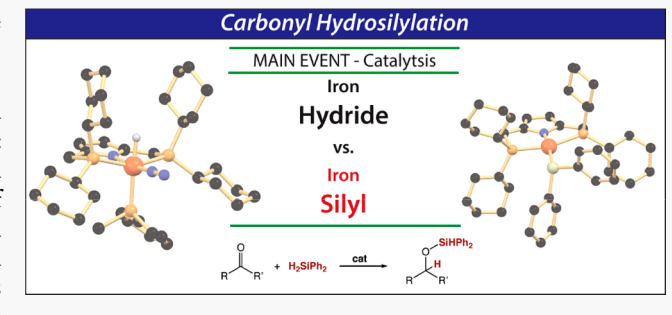
ACCESS I

Metrics & More

Article Recommendations

Supporting Information

ABSTRACT: Fe(II) hydride and silyl species of the type $[Fe(X)(L)(^{Cy}PNP)]$ (X = H or SiR_3 ; $L = N_2$ and/or PMe_2Ph ; $^{Cy}PNP =$ anion of 2,5-bis(dicylcohexylphosphinomethyl)pyrrole) serve as active catalysts for the hydrosilylation of aldehydes and ketones under mild conditions. The catalytic and stoichiometric reactivity of these complexes has been scrutinized in detail and found to support disparate pathways for hydrosilylation of aldehydes involving both a canonical Chalk—Harrod process and a peripheral pathway, which depends upon both precatalyst and substrate selection. Hydrosilylation of ketones, by contrast, appears to proceed via a common mechanism involving an iron silyl species



and a peripheral pathway. The unique mechanistic framework for iron-catalyzed hydrosilylation arising from these studies stands in contrast to most previously proposed mechanisms, which feature exclusive carbonyl insertion into a Fe-H bond.

INTRODUCTION

Earth-abundant transition metal complexes remain attractive targets for the development of new hydrofunctionalization catalysts. This popularity derives from both the promise of more sustainable catalyst systems and the unique reactivity displayed by 3d metal compounds, which in many cases diverges from that of their precious metal counterparts. Hydrosilylation, in particular, has witnessed a wealth of new catalyst designs in recent years incorporating 3d metals. These systems feature a variety of ligand architectures and have resulted in new catalysts that display both excellent activity and selectivity across a range of unsaturated substrates. In the area of carbonyl hydrosilylation, iron has proven especially efficacious, and examples of well-defined systems continue to be reported.

Among the proposed mechanisms for hydrosilylation of aldehydes and ketones, two basic frameworks are typically put forward (Scheme 1). In the first pathway, referred to as the Chalk–Harrod mechanism, carbonyl activation is accomplished via migratory insertion into a metal–hydride bond generating an alkoxide intermediate. Subsequent reductive elimination forges the Si–O bond giving rise to the silylether product. In the second mechanism, insertion of the carbonyl moiety occurs into a metal–silyl species, M–SiR₃, to generate a siloxyalkyl species as the key intermediate. In this case, C–H reductive elimination leads to generation of product. Beyond these two canonical pathways, other mechanisms featuring silylene active species and peripheral substrate association have also been put forward. By and large, however, the greatest share of mechanistic proposals for iron-

catalyzed carbonyl functionalization make use of the Chalk–Harrod mechanism. Consequently, iron hydrides have traditionally been the focus of mechanistic studies, with a few notable exceptions. 31,32

Efforts to interrogate the mechanisms of iron-catalyzed hydrosilylation have been buoyed by the use of pincer ligands, which often permit isolation of otherwise reactive species such as iron hydrides.³³ In one example, Guan and co-workers synthesized the iron hydride complex, [Fe(H)- $(PMe_3)_2(POCOP)$ (POCOP = anion of 2,6- $(^iPr_2PO)C_6H_4$), which was active for both aldehyde and ketone hydrosilylation. 19 Initial mechanistic experiments demonstrated no role for the hydride moiety during catalysis. However, a subsequent DFT study of the catalyst system supported carbonyl insertion into the Fe-H as the key step. 34 In another example, Gade and co-workers examined the mechanism of ketone hydrosilylation by a series of highly active iron carboxylate precatalysts containing an NNN boxmi pincer.35 Here again, an iron hydride was implicated as the key active species being formed via reduction of the carboxylate precatalyst. Unfortunately, observation or characterization of this hydride species was unsuccessful even with isotopic labeling.

Received: December 8, 2021 Published: February 7, 2022





Scheme 1. Canonical Mechanisms for Catalytic Carbonyl Hydrosilylation

In contrast to iron hydrides, well-defined silyl species have not received the same deal of scrutiny when it comes to carbonyl hydrosilylation.³⁶ The reactivity of such species might be envisioned to follow the modified Chalk—Harrod pathway shown in Scheme 1. Indeed, this mechanism has been proposed for several first-row transition metal pincer compounds,^{37–39} but mechanistic investigations with iron remain scarce, including the stabilization of intermediates. Herein we describe the catalytic activity and mechanistic investigation of a series of iron pincer complexes containing silyl ligands. The complexes are supported by a pyrrole-based PNP pincer ligand,⁴⁰ which is capable of stabilizing several potential intermediates along the catalytic pathway. We present evidence in support of divergent mechanistic pathways depending on the precatalyst employed and the substrate.

RESULTS

Catalytic Reactivity. Previously, we have reported the synthesis and characterization of several mechanistically relevant iron(II) pincer compounds containing both hydride and silyl ligands. On the basis of the observation that the iron hydride compound, $[FeH(PMe_2Ph)(N_2)(^{Cy}PNP)]$ (1), reacts with silanes to afford silyl complexes (eq 1), we surmised that such Fe-SiR₃ species, 2–4, were likely active intermediates along the catalytic cycle for carbonyl hydrosilylation. Accordingly, we began our investigations by examining both hydride 1 as well as silyls 2–4 as precatalysts for the hydrosilylation of benzaldehyde with different silanes.

Compounds 1 and 2 are both competent precatalysts for hydrosilylation of benzaldehyde at room temperature (Table 1, entries 1 and 2). Compound 2 appears to be a more active and efficient catalyst than 1 when employing diphenylsilane (Table 1, entry 1 vs 2), as reactions with 2 appear complete within the time of observation. Lowering the catalyst loading of 2 results in slightly depressed yields (Table 1, entries 5 and 6) although the overall efficacy remains high. By contrast, increasing the steric bulk of the silane moiety leads to a decrease in activity, requiring elevated temperatures and/or extended reaction time to give comparable yields (Table 1, entries 3 and 4). The bulkiest silane examined, triphenylsilane, failed to produce

Table 1. Catalytic Hydrosilylation of Benzaldehyde Employing Compounds 1–4^a

entry	cat.	mol %	$\mathrm{HSi}\underline{\mathrm{R}}\mathrm{Ph}_2$	yield ^b	time
1	1	2	Н	80	15 m
2	2	2	Н	98	<1 m
3	3	2	F	92	10 m
4	4	2	Me	84	10 h ^c
5	2	1	Н	90	<5 m
6	2	0.5	Н	86	<5 m
7	2	2	Ph	n.r.	$2 h^c$

^aGeneral conditions: Benzaldehyde (1 equiv), H(R)SiPh₂ (1.1 equiv), 5.0 μmol of 1,3,5-trimethoxybenzene (internal standard), and 400 μL of benzene- d_6 at room temperature. ^bYield determined by ¹H NMR integration against internal standard. ^cReaction mixture heated to 70 °C.

product in reactions catalyzed by **2**, consistent with our earlier inability to generate the corresponding silyl complex. ⁴²

Given the efficacy observed for compound 2 in reactions of benzaldehyde, we focused on its use as a precatalyst for the hydrosilylation of other aldehyde substrates (Table 2). Hydrosilylation reactions employing diphenylsilane catalyzed by 2 result in detection of both the single and double silylether products, (ArO)SiHPh₂ and (ArO)₂SiPh₂, as judged by ¹H NMR spectroscopy. As evident from Table 2, compound 2 retains its catalytic activity across a variety of aldehydes. Electronic properties of the aldehydes do not appear to exert a significant influence as evidenced by the results with parasubstituted benzaldehyde derivatives (Table 2, entries 1-5). In addition to these derivatives, we also examined both 4-nitro and 4-dimethylamino benzaldehyde, but these substrates resulted in poor yields, likely due to functional group coordination to the metal center and/or orthogonal chemistry with the M-Si unit. In terms of steric properties, the bulk of the substrate was observed to exert a much larger influence over catalytic activity. 2-Methyl- and 2-phenylbenzaldehyde led to only moderate yields, whereas mesitaldehyde did not exhibit any turnover, even upon heating (Table 2, entry 10). Butyraldehyde also displayed lower yields, and ¹H NMR spectra of the reaction products indicated formation of multiple olefinic species as well as hydrogen gas. We have

Table 2. Aldehyde Substrate Scope with Compound 2^a

		Α	•••	В
Entry	Aldehyde	Yield ^b	A/B	Time
1	°	98	69/29	< 1 m
2		96	89/7	< 1 m
3	MeO	90	85/5	< 1 m
4	F	97	78/19	< 1 m
5	F ₃ C	88	72/16	< 1 m
6	Me ₂ N	0	0/0	15 m
7	O ₂ N	0	0/0	15 m
8		66	66/0	15 m
9	Ph	72	66/6	< 1 m
10		0	0/0	$2\mathrm{h}^c$
11		38	38/0	1 h
12		74	74/0	15 m

[&]quot;General conditions: Compound 2 (2.4 μ mol), aldehyde (121 μ mol), H₂SiPh₂ (133 μ mol, 1.1 equiv), 5.0 μ mol of 1,3,5-trimethoxybenzene (internal standard), and 400 μ L of benzene- d_6 at room temperature. ^bYield determined by ¹H NMR integration against internal standard. ^cReaction mixture heated to 80 °C.

previously described the equilibrium insertion of benzaldehyde into the Fe–Si bond of compound 2. The presence of olefinic peaks and hydrogen gas would be consistent with the insertion product of butyraldehyde and 2 undergoing β -H elimination with subsequent catalyst deactivation. Sacrificial silane could then protonate the resultant hydride to reform the active catalyst. To test this possibility, crotonaldehyde was utilized as a substrate (Table 2, entry 12). The additional unsaturation present in crotonaldehyde creates a more constrained geometry that should discourage β -H elimination. Consistent with this proposal, hydrosilylation of crotonaldehyde resulted in a nearly 2-fold enhancement in yield (Table 2, entry 11).

In addition to aldehydes, ketones were also investigated as substrates for hydrosilylation (Table 3). In general, the reaction rates for ketones were found to be significantly slower than those for aldehydes and no double hydrosilylation products were observed. Acetophenone derivatives gave moderate to high yields with precatalyst 2, whereas benzophenone did not show any reactivity. Use of cyclohexanone also resulted in high yields of the silylether product but required longer reaction time compared to acetophenone. In contrast to the results with butryaldehyde, none of the catalytic reactions employing ketones with β -H atoms displayed any appreciable formation of olefinic products as judged by ¹H NMR spectroscopy indicating minimal, if any, elimination as a competing side reaction. This result is further consistent with our prior findings that ketones do not readily insert into the Fe-Si bond of 2.42

In a final set of catalytic reactions, we examined the use of the iron hydride compound 1 for the catalytic hydrosilylation of selected substrates, focusing on those that proved recalcitrant or poor-yielding with precatalyst 2 (Table 4). These substrates include both bulky aldehydes and ketones, as well as less reactive silanes. As shown in entry 4 of Table 4, compound 1 was successful for the hydrosilylation of benzophenone in contrast to results observed for 2. Additionally, compound 1 also proved viable for the hydrosilylation of benzaldehyde employing the bulkier triphenylsilane (entry 5). These data coupled with the noted difference in reaction times when using diphenylsilane (entries 1–3) support the assertion that iron hydride (1) and iron silyl (2) precatalysts operate by two distinct mechanisms.

Mechanistic Investigations. In order to deconvolute the incongruities observed for precatalysts 1 and 2, stoichiometric reactions were undertaken to interrogate the steps in the mechanistic cycles depicted in Scheme 1. Given that compound 1 contains an Fe-H moiety, we hypothesized that it most likely operates via a standard Chalk-Harrod mechanism. Addition of stoichiometric amounts of carbonyl substrates to 1 resulted in new high-spin Fe(II) species as judged by ¹H NMR spectroscopy. We tentatively assign these species as iron alkoxide complexes, which result from migratory insertion of the carbonyl unit into the Fe-H bond of 1 (eq 2). This insertion event appears to be reversible, consistent with the documented ability of this system to undergo β -H elimination.⁴³ In line with this observation, we have been unable to isolate these putative iron alkoxide species for further characterization. However, addition of diphenylsilane to the in situ generated alkoxide compounds was observed to reform 1 and release the desired silyl ether product demonstrating the chemical competence of these species.

Table 3. Ketone Substrate Scope with Compound 2^a

Q.				SiHPh ₂
R R'	+	H ₂ SiPh ₂	2 mol% 2 benzene-d ₆	H B,

К	H, penze	rie-a ₆ R F	₹'
Entry	Ketone	Yield ^b	Time
1		86	15 m
2		88	2 h
3	MeO	59	7 h
4	/Bu	83	2 h
5	F	88	15 m
6	Br	79	15 m
7	F ₃ C	72	10 m
8	CF ₃	86	1.5 h
9		0	2 h ^c
10		89	2 h

^aGeneral conditions: Compound 2 (2.4 μmol), ketone (121 μmol), H_2SiPh_2 (133 μmol, 1.1 equiv), 5.0 μmol of 1,3,5-trimethoxybenzene (internal standard), and 400 μL of benzene- d_6 at room temperature. ^bYield determined by ¹H NMR integration against internal standard. ^cReaction mixture was heated to 80 °C.

Table 4. Catalytic Results for the Hydrosilylation of Selected Substrates Using Compound 1^a

Entry	Substrate	Silane	Yield ^b	Time
1		H ₂ SiPh ₂	80	15 m
2		H ₂ SiPh ₂	74	3 h
3		H₂SiPh₂	74	8 h
4		H₂SiPh₂	73	3 h
5		HSiPh ₃	67	48 h

^aGeneral conditions: Compound 1 (1.3 μmol), substrate (64 μmol), silane (1.1 equiv), 5.0 μmol of 1,3,5-trimethoxybenzene (internal standard), and 400 μL of benzene- d_6 at room temperature. ^bYield determined by ¹H NMR integration against internal standard.

To further probe the intermediacy of putative iron alkoxides, the phenoxide complex, $[Fe(OPh)(Py)(^{Cy}PNP)]$ (5), was synthesized as shown in eq 3.

$$\begin{array}{c|cccc}
PCy_2 & & & & PCy_2 \\
N - Fe - CI & & & & N - Fe - OPh \\
PCy_2 & & & & PCy_2
\end{array}$$

$$\begin{array}{c|ccccc}
PCy_2 & & & & PCy_2 \\
N - Fe - OPh & & & PCy_2
\end{array}$$

$$\begin{array}{c|cccc}
PCy_2 & & & & PCy_2
\end{array}$$

Magnetic susceptibility measurements on 5 gave a $\mu_{\rm eff}$ of 4.6 $\mu_{\rm B}$, consistent with high-spin iron(II). Likewise, $^1{\rm H}$ NMR spectra appeared highly broadened akin to those observed for aldehyde insertion into 1. The structure of 5 is displayed in Figure 1 and demonstrates a square-pyramidal geometry akin to that of the chloride complex, [FeCl(py)($^{\rm Cy}$ PNP)]. 41 The bond lengths observed for the compound are further consistent with a high-spin ferrous center.

Stoichiometric reactions of **5** with diphenylsilane resulted in a mixture of **2**, $HSi(OPh)Ph_2$, and an unknown paramagnetic species that we tentatively assign as the new silyl species, $[Fe(Si\{OPh\}Ph_2)(^{Cy}PNP)]$. A logical sequence of reactions leading to this outcome is depicted in Scheme 2. Compound **5** initially reacts with diphenylsilane to produce a mixture of the bimetallic iron hydride, $[Fe(\mu-H)(^{Cy}PNP)]_2$ (**6**), and the corresponding silyl ether, PhOSiHPh₂. Subsequent reaction of **6** with either unreacted diphenylsilane or PhOSiHPh₂ then produces the observed product mixture. To clarify this reaction pathway, we examined use of $HSiFPh_2$, which cannot undergo reaction at a second Si-H bond. Addition of $HSiFPh_2$ to **5** resulted in clean formation of **6** and the silyl ether PhOSiFPh₂ (Scheme 2), consistent with the pathway proposed for diphenylsilane. Together, these results further demonstrate

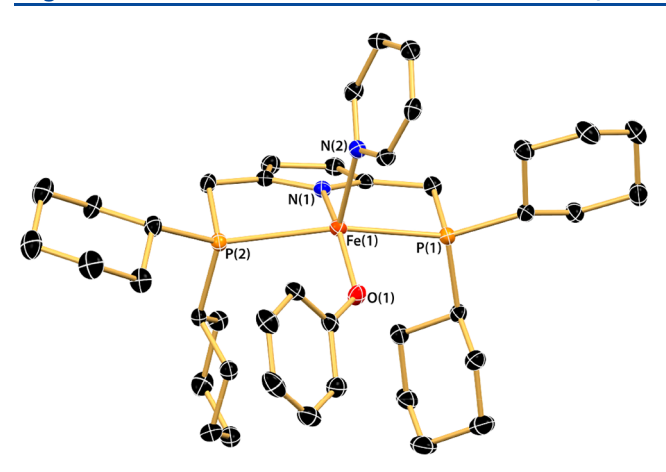


Figure 1. Thermal ellipsoid (50%) rendering of the solid-state structure of compound **5.** Hydrogen atoms omitted for clarity. Selected bond lengths (Å) and angles (deg): Fe(1)-O(1)=1.918(2), Fe(1)-N(2)=2.142(3), Fe(1)-N(1)=2.045(3), $Fe(1)-P_{avg}=2.603(1)$, N(1)-Fe(1)-O(1)=154.22(11), P(1)-Fe(1)-P(2)=147.74(3), N(2)-Fe(1)-O(1)=101.21(10).

Scheme 2. Reactivity of Compound 5 with Silanes

that iron alkoxides can serve as viable intermediates along the hydrosilylation pathway.

Turning our consideration from iron alkoxides to iron silyls, we next examined the chemistry of ${\bf 2}$ in more detail. Our previous work demonstrated an equilibrium insertion of benzaldehyde into the Fe–Si bond of ${\bf 2}$ (eq 4).

The resulting Fe- β -siloxyalkyl (A) is the expected intermediate in the modified Chalk—Harrod mechanisms shown in Scheme 1. We attempted stoichiometric addition of diphenylsilane to *in situ* generated siloxyalkyl species A to determine if it produces the expected silyl ether product. Unfortunately, these reactions did not result in the rapid formation of silylether as would be required by the catalytic results. Instead, formation of the silylether took several hours as judged by NMR spectroscopy and was accompanied by several unidentified side products. This result does not support a role for carbonyl insertion into the Fe—Si bond for catalytic reactions initiated by 2. Instead, the sluggish reactivity observed with the siloxyalkyl species suggests that it much more likely represents an off-cycle species. In further support of this idea, we find that the order of

addition of aldehyde is critically important to catalytic reactions employing 2. Addition of benzaldehyde to mixtures of 2 and diphenylsilane results in immediate product formation as judged by ¹H NMR spectroscopy. However, if diphenylsilane is added to a mixture of 2 and benzaldehyde, then hydrosilylation yields are greatly reduced, and the reaction requires several hours to reach full consumption of aldehyde. These observations reflect formation of the siloxyalkyl species A via initial reaction of 2 with aldehyde, which subsequently impedes catalytic turnover.

Given the requirement for the addition of silane to 2 prior to aldehyde, we were curious about the interactions between iron silyl precatlaysts 2 and 3 and their respective silanes (H_2SiPh_2) and $HFSiPh_2$). In prior work, we demonstrated the formation of iron silyls from 1 and silanes. We also highlighted the reversibility of the reaction in the presence of H_2 . Not examined previously was the role of molecular nitrogen (N_2) , which binds to both 1 and the silyl species 2–4. We have now examined the reaction of silanes with degassed solutions of 2 and 3 (eq 5).

Surprisingly, these reactions displayed equilibrium formation of bridging iron hydride 6, which is in direct contradiction to what we have observed under a nitrogen atmosphere. These results therefore raise the possibility that hydride 6 is generated in small quantities during turnover and serves as the active catalyst, as opposed to an iron silyl species.

To test the possibility that 6 acts as the true active species in reactions employing iron silyls 2-4, its behavior under conditions that more closely mimic catalysis was next examined (eq 6).

Under ca. 1 bar of N_2 , reaction of 10 equiv of H_2SiPh_2 with 6 led to an equilibrium mixture of 2 and 6. Increasing the amount of diphenylsilane to 20 equiv (corresponding to 5 mol % catalyst loading) led to an essentially complete formation of 2 as judged by NMR. Thus, in the presence of large excesses of silane under an N2 atmosphere, 6 is rapidly consumed to form 2. Formation of 6 under catalytic conditions is therefore unlikely, arguing against its intermediacy. Furthermore, the rapid rates of aldehyde hydrosilylation observed with 2 are incompatible with 6 serving as the active species as it would only be present in very small quantities. Instead, we favor an alternate mechanism for reactions employing iron silyl precatlysts 2-4. This mechanism likely involves peripheral reactivity, where the Fe-SiR₃ moiety interacts with the Si-H bond of the substrate priming it for reactivity with aldehyde or ketone (vide infra).

The stoichiometric reactions described above provide evidence for the involvement of different mechanistic pathways as a function of precatalyst. To help validate this proposal we next looked at linear free energy relationships for aldehyde hydrosilylation with both iron hydride and iron silyl species. Due to the observation of single and double hydrosilylation products in reactions employing diphenylsilane (Table 2), HSiFPh₂ was selected as the silane substrate. Accordingly, complex 3 was used in place of 2 as the silyl precatalyst to ensure consistency with the silane. Relative rates of hydrosilylation were determined from product ratios obtained from competition reactions for a series of substituted benzaldehyde derivatives (Figure 2). Both catalyst systems were found to

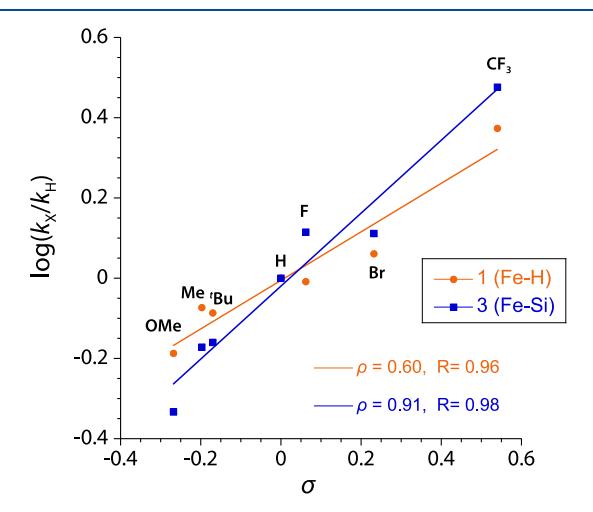


Figure 2. Hammett correlation for the hydrosilylation of *para*-substituted benzaldehyde derivatives with HSiFPh₂ catalyzed by 1 (orange) and 3 (blue). Values of $\log(k_{\rm X}/k_{\rm H})$ were determined by product ratios from competition experiments.

display a positive slope indicating the buildup of negative charge in the transition state. However, the ρ values for the two catalyst systems (0.60 and 0.91 for 1 and 3, respectively) were found to show significant differences, consistent with distinct mechanistic pathways for the two precatalysts.

Similar examination of ketone hydrosilylation using acetophenone derivatives produced the Hammett correlation plots shown in Figure 3. In contrast to aldehydes, hydrosilylation of ketones by both 1 and 3 shows a nearly identical correlation for both precatalysts.

The similarity of both Hammett correlations for precatalysts 1 and 3 suggests that one mechanism dominates when ketones are used as substrates. This situation contrasts results with aldehydes, where both catalytic studies and the Hammett plots suggest two different mechanisms are at play depending upon the precatalyst employed. The identity of the substrate (aldehyde versus ketone) therefore plays a significant role in selecting for the operative hydrosilylation pathway. In the case of aldehydes, equilibrium insertion of benzaldehyde into 1 is likely rapid and able to compete with protonation by diphenylsilane to give 2. As such the Fe-H unit remains intact and can catalyze hydrosilylation via a Chalk-Harrod mechanism. By contrast, reactions employing 2 have no means of rapidly regenerating 1 during catalytic turnover and therefore must proceed by a different mechanism. The sluggish reactivity observed for intermediate A argues against a modified Chalk-Harrod process; therefore, reactions with

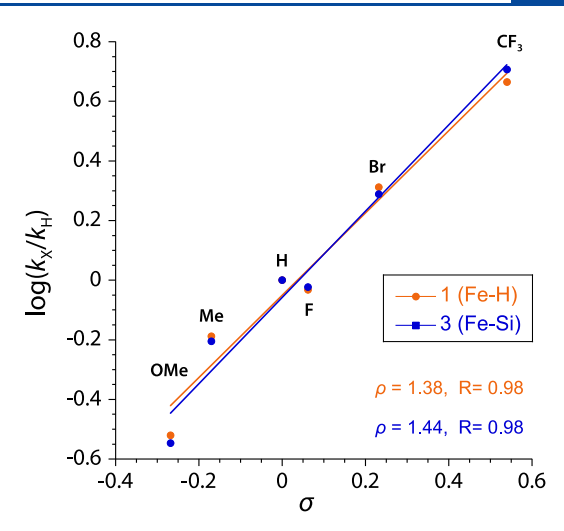


Figure 3. Hammett correlation for the hydrosilylation of *para*-substituted acetophenone derivatives with HSiFPh₂ catalyzed by 1 (orange) and 3 (blue). Values of $\log(k_{\rm X}/k_{\rm H})$ were determined by product ratios from competition experiments.

precatalyst 2 most likely proceed by a peripheral process. In the case of ketones, insertion of the carbonyl unit into the Fe—H bond of 1 is considerably slower providing an opportunity for formation of 2 (eq 1). Consequently, both precatalysts operate by a common mechanism featuring Fe—Si species akin to aldehyde hydrosilylation by 2. When 1 is employed, however, the molecular hydrogen generated by reaction with silane ensures that some quantity of both Fe—H and Fe—Si remain present in solution. Thus, in cases where hydrosilylation is not observed with the silyl precatalyst (e.g., benzophenone), precatalyst 1 is capable of defaulting to a Chalk—Harrod-type pathway. This mechanistic proposal is in good agreement with the disparate reactivity between 1 and 2 with select substrates as seen in Table 4.

The Hammett plots for both aldehyde and ketone hydrosilylation displayed above demonstrate that substrate substituents exert an effect on the rate of the catalytic reaction, but they do not provide definitive information regarding the nature of the turnover-limiting step, nor do they reveal to what extent other factors may influence overall catalytic efficacy. We were therefore curious to examine the kinetics of the hydrosilylation reaction to provide further clarity. The rapid nature of the hydrosilylation reaction with benzaldehyde derivatives made kinetic monitoring of such reactions challenging, so efforts were directed toward ketones. For operational simplicity, we elected to monitor the reaction of 4fluoroacetophenone with diphenylsilane by ¹⁹F NMR spectroscopy. A representative reaction profile for both 1 and 2 as precatalysts can be found in the Supporting Information. When 1 was used, both ketone and silane were added simultaneously to avoid the formation of 2. For reactions employing precatalyst 2, silane was added before 4-fluoroacetophenone. Kinetic profiles for both processes are complex, so the initial rate of catalyst 1 was taken as the tangent of the initial 630 s of the reaction. Catalyst 2 proved more rapid, and the initial rate was determined in similar fashion using the first 80 s of the reaction.

Reaction component dependences were investigated by monitoring the change in initial rate upon variation in the concentrations of each reactant. Catalyst loading was examined first. Increasing the concentration of both 1 and 2 resulted in a

Scheme 3. Mechanistic Proposal for Catalytic Hydrosilylation by CyPNPFe

positive dependence on the initial rates, consistent with the turnover-limiting step involving the iron catalyst (see the Supporting Information). In similar fashion, variation in the concentration of acetophenone also demonstrated positive dependences for both 1 and 2. In the case of both catalyst and acetophenone concentration, fits of the initial rate data to power functions suggested noninteger dependences for several reactants (see the Supporting Information). We believe these values reflect the multiple complex equilibria at play during catalytic turnover and are not indicative of a single turnover-limiting elementary step (vide infra).

In contrast to both catalyst and acetophenone concentration, varying the amount of diphenylsilane was observed to lead to a minor slowing of the initial rate for both precatalysts. This result is surprising given that typical mechanistic proposals for carbonyl hydrosilylation feature a positive dependence on silane concentration. For example, Gade and co-workers observed a first-order dependence on silane concentration with the Fe boxmi pincer system, consistent with a Chalk-Harrod-type mechanism involving rate-determining addition of silane to an intermediate iron alkoxide.³⁵ In our system, we propose that the apparent negative dependence on silane may stem from the ability of active species 2-silane (vide infra) to react with additional silane leading to degenerate silyl exchange. In this way, silane competes directly with incoming substrate accounting for the negative dependence. In support of this conjecture, addition of excess H₂SiPh₂ to compound 4 in the absence of carbonyl substrate was found to rapidly generate a mixture of 2 and 4 (eq 7).

A final consideration in the chemistry of both compounds 1 and 2 is the role of molecular nitrogen and phosphine during catalytic turnover. Having established the proclivity of both species to bind N_2 , we anticipate that the rate of hydrosilylation with both precatalysts will show a minor negative dependence on N_2 concentration. However, due to the challenge of reproducibly altering the partial pressures of N_2

for these multicomponent reactions, we have not performed such experiments at this time. Regarding the role of phosphine, we have examined catalysis using 2 in the presence of PMe₂Ph. We have previously demonstrated that phosphine binds to the silyl species, 2, to generate 2·PMe₂Ph. 42 Indeed, the phosphine adduct can be isolated from the addition of H₂SiPh₂ to 1. ¹H and ³¹P NMR spectra of 2·PMe₂Ph and 2, however, are identical at ambient temperature indicating equilibrium association of PMe₂Ph to 2 on a time scale faster than that of the NMR. To test the possibility that PMe₂Ph serves as a catalytic inhibitor, kinetic experiments were also performed with 2·PMe₂Ph. Initial rates for 2·PMe₂Ph were slower than those of 2, confirming that PMe₂Ph does have an inhibitory effect on catalysis. Moreover, the presence of PMe₂Ph brings the initial rate of catalysis by 2.PMe2Ph in line with that of 1, further consistent with a unified peripheral mechanism for both precatalysts in the case of ketone hydrosilylation. Last, we also examined the kinetics of the bridging hydride complex, 6, to rule out the possibility that it forms in small quantities when 2 is exposed to H₂SiPh₂ and serves as the active catalyst. Initial rates with compound 6 were found to be the slowest of the complexes examined and it is therefore unlikely that this species plays a significant role in catalysis.

DISCUSSION

Given the results of both the stoichiometric experiments and kinetics trials presented above, we propose a mechanism for the iron-catalyzed hydrosilylation of aldehydes and ketones depicted in Scheme 3. In the case of aldehyde hydrosilylation by precatalyst 1, equilibrium insertion of the carbonyl unit into the Fe-H bond is relatively facile and produces an intermediate iron alkoxide species. Incoming silane then performs a σ -bond metathesis to re-form 1 and release the silylether product according to a standard Chalk-Harrod-type process. By contrast, precatalyst 2 is unlikely to operate by a similar mechanism since it lacks an Fe-H or access thereto under the reaction conditions. Instead, we observe that addition of aldehyde can lead to equilibrium insertion into the Fe-Si bond to form a Fe- β -siloxyalkyl species. Such a pathway would correlate with a modified Chalk-Harrod mechanism as shown in Scheme 1. However, in the present system these siloxyalkyl species are not kinetically competent

as demonstrated by the requirement that reactions initiated with 2–4 be premixed with silane prior to addition of aldehyde. This fact therefore supports an alternative mechanism for precatalyst 2 involving formation of a silyl–silane adduct (2·silane). Peripheral reaction of carbonyl substrates with the activated silane complex then permits σ -bond metathesis to occur in the outer-sphere of the Fe center. Unlike the peripheral mechanism reported by Driess and Oestreich, however, we believe the metal center activates the silane as opposed to the carbonyl substrate for further reactivity. In this way, the present system is more akin to the Ru phosphinoborane catalyst reported by Tilley, which was demonstrated to react with ketones through activated η^3 -silane adducts.

Attempts to observe the silane adduct, **2·silane**, by NMR spectroscopy have thus far been unsuccessful most likely due to the equilibrium nature of silane association (*vide supra* **2·PMe₂Ph**). Moreover, the activated adduct is likely to readily engage in silyl exchange, further confounding attempts to observe it spectroscopically. Such a consideration could explain the apparent inverse silane dependence observed for ketone hydrosilylation. In addition, both N₂ and free phosphine will lead to competing equilibria with silane association accounting for the noninteger dependencies observed in kinetics experiments and the observed slowing of ketone hydrosilylation by **2** in the presence of PMe₂Ph.

For ketone hydrosilylation, the Hammett analysis points to a single mechanism for both precatalysts ${\bf 1}$ and ${\bf 2}$. Given that carbonyl insertion into the Fe–H bond of ${\bf 1}$ is significantly slower on steric grounds, protonation by silane is likely to be competitive giving rise to an iron silyl species akin to ${\bf 2}$ under catalytic conditions. Hydrosilylation of ketones is therefore more likely to operate via a peripheral mechanism featuring a Fe–Si species for both precatalysts ${\bf 1}$ and ${\bf 2}$. In the case of precatalyst ${\bf 1}$, the remaining equivalent of ${\bf H}_2$ formed by protonation of the hydride permits the regeneration of ${\bf 1}$, which is relevant for those substrates like benzophenone that show no turnover with precatalyst ${\bf 2}$.

The mechanistic framework in Scheme 3 also explains many of the substrate preferences observed for the catalyst system. Steric requirements of both the carbonyl substrate and silane affect the overall catalytic efficacy, with bulkier groups disfavoring both the formation of **2·silane** and the corresponding transition state for hydrosilylation. Likewise, aliphatic aldehydes and ketones present the possibility for unproductive β -H elimination from insertion products involving the Fe—Si bond.

CONCLUSIONS

In this contribution, we sought to probe the role of iron silyl species in carbonyl hydrosilylation with a well-defined pincer system. Given that mechanistic proposals for hydrosilylation are discussed frequently with little direct evidence for discrete catalytic steps, we chose to examine a series of iron complexes of relevance to both Fe–H and Fe–Si driven mechanisms (Scheme 1).

Stoichiometric reactivity of iron hydrides with aldehydes established the 1,2-migratory insertion of carbonyl moieties into the Fe–H bond to form an Fe alkoxide followed by subsequent σ -bond metathesis to reform the Fe hydride. The steric properties of both the carbonyl moiety and silane used influence whether a Chalk–Harrod or peripheral mechanism is operative, and both may be operative simultaneously when Fe

hydrides are employed. In the case of iron silyl species, 2,1-insertion of aldehydes into the Fe–Si bond produces a silyoxyalkyl intermediate, but the subsequent σ -bond metathesis required to close the catalytic cycle was not kinetically competent. Instead, initial reaction of the iron silyl species with silane is required to observe hydrosilylation at a comparable rate to what was observed catalytically.

Kinetic investigations of ketone hydrosilylation support a common mechanism for both hydride and silyl precatalysts. This proposal was further bolstered by Hammet studies, which demonstrated nearly identical ρ values for the two catalysts systems. In total, these data are consistent with a peripheral mechanism (Scheme 3) which hinges upon the reaction of ketone or aldehyde with an Fe-silane active species.

On a final note, many mechanistic proposals for Fe-catalyzed hydrofunctionalizations of polar substrates propose the intermediacy of iron hydrides. In this study, we have provided strong evidence for an alternative picture, in which the active species under certain conditions may feature an Fe-heteroatom bond. Furthermore, we have demonstrated the importance of competitive side-reactions of the active catalyst that do not alter the overall product distribution but play an important role in the observed kinetics. Such reactions are often dismissed, but they likely feature prominently in catalysis by earth-abundant metal systems where energy barriers to off-pathway reactions may be much lower than those for precious metals.

EXPERIMENTAL SECTION

General Comments. All manipulations were performed under an atmosphere of purified nitrogen gas using a Vacuum Atmospheres glovebox. Tetrahydrofuran, diethyl ether, pentane, and toluene were purified by sparging with argon and passage through two columns packed with 4 Å molecular sieves and activated alumina (THF). $^1\mathrm{H}$ NMR spectra were recorded on a Bruker spectrometer operating at 300 or 500 MHz ($^1\mathrm{H}$) in benzene- d_6 unless otherwise noted and referenced to the residual protium resonance of the solvent (δ 7.16 ppm). $^{19}\mathrm{F}$ NMR spectra were recorded at 470 MHz and referenced automatically using the $^2\mathrm{H}$ lock frequency. Magnetic susceptibility measurements were performed in solution using Evans' method 46 without a solvent correction using reported diamagnetic corrections. 47 Elemental analyses were performed by the CENTC facility at the University of Rochester.

Materials. Compounds 1–4 and HSiFPh₂ were prepared according to published procedures. ^{42,48} All other reagents were purchased from commercial suppliers and used as received.

Crystallography. Crystals of 5 suitable for X-ray diffraction were mounted, using Paratone oil, onto a nylon loop. All data were collected at 98(2) K using a Rigaku AFC12/Saturn 724 CCD fitted with Mo K α radiation (λ = 0.71075 Å). Low-temperature data collection was accomplished with a nitrogen cold stream maintained by an X-Stream low-temperature apparatus. Data collection and unit cell refinement were performed using CrystalClear software. Pata processing and absorption correction, giving minimum and maximum transmission factors, were accomplished with CrysAlisPro⁵⁰ and SCALE3 ABSPACK, 1 respectively. The structure, using Olex2, was solved with the ShelXT structure solution program using direct methods and refined (on F^2) with the ShelXL refinement package using the full-matrix, least-squares techniques. S3,54 All nonhydrogen atoms were refined with anisotropic displacement parameters. All hydrogen atom positions were determined by geometry and refined by a riding model.

[Fe(OPh)(Py)(^{Cy}PNP)], **5.** A flask was charged with 0.256 g (0.390 mmol) of [FeCl(py)(^{Cy}PNP)] and 5 mL of THF. To the golden yellow solution, 0.045 g (0.39 mmol) of NaOPh as a solid was added in one portion. The solution immediately became red-orange in color.

The reaction mixture was allowed to stir for 2 h at room temperature. All volatiles were removed in vacuo, and the red residue was extracted into toluene and filtered through a pad of Celite. The toluene solution was evaporated to dryness to give a red residue. The residue was dissolved in a minimal amount of heptane, filtered, and the solution set aside at $-30~^{\circ}\mathrm{C}$ for 24 h. During this time the desired material precipitated as 0.207 g (74%) of green crystals. Crystals suitable for X-ray diffraction were grown from a concentrated heptane solution at room temperature. Mp: 124–127 °C. $\mu_{\mathrm{eff}}=4.6(4)~\mu_{\mathrm{B}}.$ NMR (300 MHz): $^{1}\mathrm{H}~\delta$ 45.2, 44.0, 43.7, 31.4, 25.5, 12.4, 8.0, 2.2, 2.1, -0.1, -1.6, -3.6, -8.0, -12.6, -25.8. Anal. Calcd for $\mathrm{C_{41}H_{60}FeN_2OP_2\cdot 1/2C_7H_{16}}$: C, 69.88; H, 8.96; N, 3.66. Found: C, 69.70; H, 9.13; N, 3.44. Elevated C and H and depressed N values are consistent with residual amounts of heptane in the lattice.

General Procedure for Hydrosilylation Reactions. An NMR tube was charged with 0.5–2.4 μ mol of catalyst as a solution in benzene- d_6 , 55–133 μ mol of H₂SiPh₂, and 5.0 μ mol of 1,3,5-trimethoxybenzene as an internal standard. Ketones and aldehydes were added as 10 μ L aliquots (55–121 μ mol) for neat liquid substrates or 100 μ L aliquots of either 50 or 100 mM solutions in benezene- d_6 (50–100 μ mol) for solid substrates. The final volume of the NMR tube was brought to 400 μ L with additional benzene- d_6 . The yield of silyl ether was determined by NMR integration and each experiment repeated a minimum of 2 times.

General Procedure for Hammett Experiments with Aldehydes. An NMR tube was charged with 2.0 μ mol of catalyst 1 or 3 and 98 μ mol of HSiFPh₂. To this mixture was added an equimolar amount of benzaldehyde and p-substituted benzaldehyde (each 98 μ mol) as a solution in benzene- d_6 . The final volume of the NMR tube was then brought to 400 μ L with additional benzene- d_6 . In the case of 1, both silane and ketone substrates were added simultaneously to avoid formation of 3. Relative rate constants were determined by NMR integration of the corresponding silyl ether products. Each experiment was conducted a minimum of 3 times.

General Procedure for Hammett Experiments with Ketones. An NMR tube was charged with 1.6 μ mol of catalyst 1 or 3 and 86 μ mol of HFSiPh₂. To this mixture was added an equimolar amount of acetophenone and p-substituted acetophenone (each 86 μ mol) as a solution in benzene- d_6 . The final volume of the NMR tube was then brought to 400 μ L with additional benzene- d_6 . In the case of 1, both silane and ketone substrates were added simultaneously to avoid formation of 3. Relative rate constants were determined by NMR integration of the corresponding silyl ether products. Each experiment was conducted a minimum of 3 times.

General Procedure for Kinetics Experiments. An NMR tube was charged with 4.1–8.2 μ mol of catalyst 1 or 2, 226–905 μ mol of H₂SiPh₂, 64 μ mol of 1,4-bis(trifluoromethyl)benzene as an internal standard, and sufficient benzene d_6 to achieve a final solution volume of 500 μ L after addition of 4-fluoroacetophenone. The tube was capped with a rubber septum. After initial lock and shim of the sample, 206–659 μ mol of 4-fluoroacetophenone was injected into the tube via the septum. In the case of 1, both silane and ketone were added simultaneously after initial lock and shim. Data acquisition was commenced immediately after injection of substrate. Each kinetics trial was conducted a minimum of 2 times.

ASSOCIATED CONTENT

Supporting Information

The Supporting Information is available free of charge at https://pubs.acs.org/doi/10.1021/acs.organomet.1c00682.

NMR data, kinetic plots, tables of crystallographic data and refinement parameters (PDF)

Accession Codes

CCDC 1882439 contains the supplementary crystallographic data for this paper. These data can be obtained free of charge via www.ccdc.cam.ac.uk/data_request/cif, or by emailing data request@ccdc.cam.ac.uk, or by contacting The Cam-

bridge Crystallographic Data Centre, 12 Union Road, Cambridge CB2 1EZ, UK; fax: +44 1223 336033.

AUTHOR INFORMATION

Corresponding Author

Zachary J. Tonzetich — Department of Chemistry, University of Texas at San Antonio (UTSA), San Antonio, Texas 78249, United States; orcid.org/0000-0001-7010-8007; Email: zachary.tonzetich@utsa.edu

Authors

C. Vance Thompson – Department of Chemistry, University of Texas at San Antonio (UTSA), San Antonio, Texas 78249, United States

Hadi D. Arman – Department of Chemistry, University of Texas at San Antonio (UTSA), San Antonio, Texas 78249, United States

Complete contact information is available at: https://pubs.acs.org/10.1021/acs.organomet.1c00682

Notes

The authors declare no competing financial interest.

ACKNOWLEDGMENTS

The authors thank the Welch Foundation (AX-1772) for financial support of this work. NMR and X-ray crystallography facilities at UTSA are supported by grants from the National Science Foundation (CHE-1625963 and CHE-1920057). The CENTC Elemental Analysis Facility is supported by NSF (CHE-0650456).

REFERENCES

- (1) Wei, D.; Darcel, C. Iron Catalysis in Reduction and Hydrometalation Reactions. *Chem. Rev.* **2019**, *119*, 2550–2610.
- (2) Chirik, P. J.; Morris, R. H. Getting Down to Earth: The Renaissance of Catalysis with Abundant Metals. *Acc. Chem. Res.* **2015**, 48, 2495–2495.
- (3) Uvarov, V. M.; de Vekki, D. A. Recent progress in the development of catalytic systems for homogenous asymmetric hydrosilylation of ketones. *J. Organomet. Chem.* **2020**, 923, 121415.
- (4) Darcel, C.; Sortais, J.-B.; Wei, D.; Bruneau-Voisine, A. Iron-, Cobalt-, and Manganese-Catalyzed Hydrosilylation of Carbonyl Compounds and Carbon Dioxide. In *Non-Noble Metal Catalysis*; Klein Gebbink, R. J. M., Moret, M.-E., Eds.; Wiley-VCH, 2019; pp 241–264.
- (5) Bhunia, M.; Sreejyothi, P.; Mandal, S. K. Earth-abundant metal catalyzed hydrosilylative reduction of various functional groups. *Coord. Chem. Rev.* **2020**, *405*, 213110.
- (6) Sharma, A.; Trovitch, R. J. Phosphorous-substituted redox-active ligands in base metal hydrosilylation catalysis. *Dalton Trans.* **2021**, *50*, 15973–15977.
- (7) Zhang, M.; Zhang, A. Iron-catalyzed hydrosilylation reactions. *Appl. Organomet. Chem.* **2010**, 24, 751–757.
- (8) Deng, Q. H.; Melen, R. L.; Gade, L. H. Anionic chiral tridentate N-donor pincer ligands in asymmetric catalysis. *Acc. Chem. Res.* **2014**, 47, 3162–3173.
- (9) Raya-Barón, Á.; Oña-Burgos, P.; Fernández, I. Iron-Catalyzed Homogeneous Hydrosilylation of Ketones and Aldehydes: Advances and Mechanistic Perspective. *ACS Catal.* **2019**, *9*, 5400–5417.
- (10) Nylund, P. V. S.; Ségaud, N. C.; Albrecht, M. Highly Modular Piano-Stool N-Heterocyclic Carbene Iron Complexes: Impact of Ligand Variation on Hydrosilylation Activity. *Organometallics* **2021**, *40*, 1538–1550.
- (11) Lou, K.; Zhou, Q.; Wang, Q.; Fan, X.; Xu, X.; Cui, C. CpFe(CO)2 anion-catalyzed highly efficient hydrosilylation of ketones and aldehydes. *Dalton Trans.* **2021**, *50*, 11016–11020.

- (12) Chang, G.; Zhang, P.; Yang, W.; Xie, S.; Sun, H.; Li, X.; Fuhr, O.; Fenske, D. Pyridine N-oxide promoted hydrosilylation of carbonyl compounds catalyzed by [PSiP]-pincer iron hydrides. *Dalton Trans.* **2020**, *49*, 9349–9354.
- (13) Qi, X.; Zhao, H.; Sun, H.; Li, X.; Fuhr, O.; Fenske, D. Synthesis and catalytic application of [PPP]-pincer iron, nickel and cobalt complexes for the hydrosilylation of aldehydes and ketones. *New J. Chem.* **2018**, *42*, 16583–16590.
- (14) Lin, H.-J.; Lutz, S.; O'Kane, C.; Zeller, M.; Chen, C.-H.; Al Assil, T.; Lee, W.-T. Synthesis and characterization of an iron complex bearing a hemilabile NNN-pincer for catalytic hydrosilylation of organic carbonyl compounds. *Dalton Trans.* **2018**, *47*, 3243–3247.
- (15) Bleith, T.; Wadepohl, H.; Gade, L. H. Iron Achieves Noble Metal Reactivity and Selectivity: Highly Reactive and Enantioselective Iron Complexes as Catalysts in the Hydrosilylation of Ketones. *J. Am. Chem. Soc.* **2015**, *137*, 2456–2459.
- (16) Huang, S.; Zhao, H.; Li, X.; Wang, L.; Sun, H. Synthesis of [POCOP]-pincer iron and cobalt complexes via Csp3-H activation and catalytic application of iron hydride in hydrosilylation reactions. *RSC Adv.* **2015**, *5*, 15660–15667.
- (17) Gallego, D.; Inoue, S.; Blom, B.; Driess, M. Highly Electron-Rich Pincer-Type Iron Complexes Bearing Innocent Bis(metallylene)-pyridine Ligands: Syntheses, Structures, and Catalytic Activity. *Organometallics* **2014**, *33*, 6885–6897.
- (18) Ruddy, A. J.; Kelly, C. M.; Crawford, S. M.; Wheaton, C. A.; Sydora, O. L.; Small, B. L.; Stradiotto, M.; Turculet, L. (N-Phosphinoamidinate)Iron Pre-Catalysts for the Room Temperature Hydrosilylation of Carbonyl Compounds with Broad Substrate Scope at Low Loadings. *Organometallics* **2013**, 32, 5581–5588.
- (19) Bhattacharya, P.; Krause, J. A.; Guan, H. Iron Hydride Complexes Bearing Phosphinite-Based Pincer Ligands: Synthesis, Reactivity, and Catalytic Application in Hydrosilylation Reactions. *Organometallics* **2011**, *30*, 4720–4729.
- (20) Tondreau, A. M.; Darmon, J. M.; Wile, B. M.; Floyd, S. K.; Lobkovsky, E.; Chirik, P. J. Enantiopure Pyridine Bis(oxazoline) "Pybox" and Bis(oxazoline) "Box" Iron Dialkyl Complexes: Comparison to Bis(imino)pyridine Compounds and Application to Catalytic Hydrosilylation of Ketones. *Organometallics* **2009**, 28, 3928–3940.
- (21) Tondreau, A. M.; Lobkovsky, E.; Chirik, P. J. Bis(imino)-pyridine Iron Complexes for Aldehyde and Ketone Hydrosilylation. *Org. Lett.* **2008**, *10*, 2789–2792.
- (22) Chalk, A. J.; Harrod, J. F. Homogeneous Catalysis. II. The Mechanism of the Hydrosilation of Olefins Catalyzed by Group VIII Metal Complexes 1. J. Am. Chem. Soc. 1965, 87, 16–21.
- (23) Randolph, C. L.; Wrighton, M. S. Photochemical reactions of $(\eta^5$ -pentamethylcyclopentadienyl)dicarbonyliron alkyl and silyl complexes: reversible ethylene insertion into an iron-silicon bond and implications for the mechanism of transition-metal-catalyzed hydrosilation of alkenes. *J. Am. Chem. Soc.* **1986**, *108*, 3366–3374.
- (24) Ojima, I.; Clos, N.; Donovan, R. J.; Ingallina, P. Hydrosilylation of 1-hexyne catalyzed by rhodium and cobalt-rhodium mixed-metal complexes. Mechanism of apparent trans addition. *Organometallics* **1990**, *9*, 3127–3133.
- (25) Brookhart, M.; Grant, B. E. Mechanism of a cobalt(III)-catalyzed olefin hydrosilation reaction: direct evidence for a silyl migration pathway. *J. Am. Chem. Soc.* **1993**, *115*, 2151–2156.
- (26) Schneider, N.; Finger, M.; Haferkemper, C.; Bellemin-Laponnaz, S.; Hofmann, P.; Gade, L. H. Multiple Reaction Pathways in Rhodium-Catalyzed Hydrosilylations of Ketones. *Chem. Eur. J.* **2009**, *15*, 11515–11529.
- (27) Blom, B.; Enthaler, S.; Inoue, S.; Irran, E.; Driess, M. Electron-Rich N-Heterocyclic Silylene (NHSi)-Iron Complexes: Synthesis, Structures, and Catalytic Ability of an Isolable Hydridosilylene-Iron Complex. J. Am. Chem. Soc. 2013, 135, 6703–6713.
- (28) Metsänen, T. T.; Gallego, D.; Szilvási, T.; Driess, M.; Oestreich, M. Peripheral mechanism of a carbonyl hydrosilylation catalysed by an SiNSi iron pincer complex. *Chem. Sci.* **2015**, *6*, 7143–7149.

- (29) Zheng, G. Z.; Chan, T. H. Regiocontrolled Hydrosilation of alpha.beta.-Unsaturated Carbonyl Compounds Catalyzed by Hydridotetrakis(triphenylphosphine)rhodium(I). *Organometallics* 1995, 14, 70–79.
- (30) Smith, P. W.; Dong, Y.; Tilley, T. D. Efficient and selective alkene hydrosilation promoted by weak, double Si-H activation at an iron center. *Chem. Sci.* **2020**, *11*, 7070–7075.
- (31) Yang, J.; Postils, V.; Lipschutz, M. I.; Fasulo, M.; Raynaud, C.; Clot, E.; Eisenstein, O.; Tilley, T. D. Efficient alkene hydrosilation with bis(8-quinolyl)phosphine (NPN) nickel catalysts. The dominant role of silyl-over hydrido-nickel catalytic intermediates. *Chem. Sci.* **2020**, *11*, 5043–5051.
- (32) MacMillan, S. N.; Hill Harman, W.; Peters, J. C. Facile Si-H bond activation and hydrosilylation catalysis mediated by a nickel-borane complex. *Chem. Sci.* **2014**, *5*, 590–597.
- (33) Peris, E.; Crabtree, R. H. Key factors in pincer ligand design. *Chem. Soc. Rev.* **2018**, 47, 1959–1968.
- (34) Wang, W.; Gu, P.; Wang, Y.; Wei, H. Theoretical Study of POCOP-Pincer Iridium(III)/Iron(II) Hydride Catalyzed Hydrosilylation of Carbonyl Compounds: Hydride Not Involved in the Iridium(III) System but Involved in the Iron(II) System. *Organometallics* **2014**, *33*, 847–857.
- (35) Bleith, T.; Gade, L. H. Mechanism of the Iron(II)-Catalyzed Hydrosilylation of Ketones: Activation of Iron Carboxylate Precatalysts and Reaction Pathways of the Active Catalyst. *J. Am. Chem. Soc.* **2016**, *138*, 4972–4983.
- (36) Whited, M. T.; Taylor, B. L. H. Metal/Organosilicon Complexes: Structure, Reactivity, and Considerations for Catalysis. *Comments Inorg. Chem.* **2020**, 40, 217–276.
- (37) Mukhopadhyay, T. K.; Flores, M.; Groy, T. L.; Trovitch, R. J. A highly active manganese precatalyst for the hydrosilylation of ketones and esters. *J. Am. Chem. Soc.* **2014**, *136*, 882–885.
- (38) Mukhopadhyay, T. K.; Rock, C. L.; Hong, M.; Ashley, D. C.; Groy, T. L.; Baik, M.-H.; Trovitch, R. J. Mechanistic Investigation of Bis (imino) pyridine Manganese Catalyzed Carbonyl and Carboxylate Hydrosilylation. *J. Am. Chem. Soc.* **2017**, *139*, 4901–4915.
- (39) Trovitch, R. J. synpacts Comparing Well-Defined Manganese, Iron, Cobalt, and Nickel Ketone Hydro-silylation Catalysts. *Synlett* **2014**, 25, 1638–1642.
- (40) Thompson, C. V.; Tonzetich, Z. J. Chapter Four Pincer ligands incorporating pyrrolyl units: Versatile platforms for organometallic chemistry and catalysis. *Adv. Organomet. Chem.* **2020**, *74*, 153–240.
- (41) Thompson, C. V.; Arman, H. D.; Tonzetich, Z. J. A Pyrrole-Based Pincer Ligand Permits Access to Three Oxidation States of Iron in Organometallic Complexes. *Organometallics* **2017**, *36*, 1795–1802.
- (42) Thompson, C. V.; Arman, H. D.; Tonzetich, Z. J. Square-Planar Iron(II) Silyl Complexes: Synthesis, Characterization, and Insertion Reactivity. *Organometallics* **2019**, *38*, 2979–2989.
- (43) Thompson, C. V.; Davis, I.; DeGayner, J. A.; Arman, H. D.; Tonzetich, Z. J. Iron Pincer Complexes Incorporating Bipyridine: A Strategy for Stabilization of Reactive Species. *Organometallics* **2017**, *36*, 4928–4935.
- (44) Pugh, D.; Wells, N. J.; Evans, D. J.; Danopoulos, A. A. Reactions of 'pincer' pyridine dicarbene complexes of Fe(0) with silanes. *Dalton Trans.* **2009**, 7189–7195.
- (45) Lipke, M. C.; Tilley, T. D. Hypercoordinate Ketone Adducts of Electrophilic η3-H2SiRR' Ligands on Ruthenium as Key Intermediates for Efficient and Robust Catalytic Hydrosilation. *J. Am. Chem. Soc.* **2014**, *136*, 16387–16398.
- (46) Sur, S. K. Measurement of magnetic susceptibility and magnetic moment of paramagnetic molecules in solution by high-field fourier transform NMR spectroscopy. *J. Magn. Reson.* **1989**, *82*, 169–173.
- (47) Bain, G. A.; Berry, J. F. Diamagnetic Corrections and Pascal's Constants. *J. Chem. Educ.* **2008**, *85*, 532–536.
- (48) Damrauer, R.; Simon, R. A.; Kanner, B. Synthesis of fluorosilanes from chlorosilanes: the use of hexafluorosilicates. *Organometallics* **1988**, *7*, 1161–1164.

- (49) CrystalClear User's Manual; Rigaku/MSC Inc., Rigaku Corporation: The Woodlands, TX, 2011.
- (50) Crys Alis Pro; Rigaku Corporation: The Woodlands, TX, 2015.
- (51) SCALE3 ABSPACK An Oxford Diffraction Program; Oxford Diffraction Ltd., 2005.
- (52) Dolomanov, O. V.; Bourhis, L. J.; Gildea, R. J.; Howard, J. A. K.; Puschmann, H. OLEX2: a complete structure solution, refinement and analysis program. *J. Appl. Crystallogr.* **2009**, *42*, 339–341. (53) Sheldrick, G. SHELXT - Integrated space-group and crystal-
- structure determination. Acta Crystallogr., Sect. A 2015, 71, 3-8.
- (54) Sheldrick, G. M. A short history of SHELX. Acta Crystallogr., Sect. A 2008, A64, 112-122.

